Integrated Efficiency of Using Nanocellulose-Nano Zero Valent Iron Composite in Water Treatment

Jian-Hui Wang,[a,b] Mohamed S. Mahmoud,[c,*] and Ahmed S. Mahmoud [d]

Water treatment using nano-materials can have a significant impact due to its surface properties. Coagulation techniques were studied by using 3 mL/L of 0.5% of different coagulants (polyacrylamide, poly aluminum chloride (PAC), ferric chloride, aluminum sulfate, and nanocellulose). Results indicated that the turbidity removal efficiency were 91.6%, 93.04%, 95.2%, 95.4%, and 99.4%, respectively. Treatment of water samples collected from the Ismailia Canal, the Damietta branch of the Nile Delta, and a wastewater treatment plant located in Cairo (Egypt) using nanocellulose fibers was studied. For the Ismailia Canal sample, the removal of turbidity, chemical oxygen demand (COD), biological oxygen demand (BOD), and phosphorous were 96%, 83.3%, 100%, and 100%, respectively. For the Damietta branch sample, the removal of turbidity, COD, BOD, and phosphorous were 87.5%, 81.3%, 88.9%, and 99.1%, respectively. For the wastewater treatment plant sample, the removal of turbidity, COD, BOD, and phosphorous were 86.4%, 91.96%, 92.86%, and 91.74%, respectively. Nanocellulose-nano zero-valent iron composite (NC-nZVI) was investigated for phosphorous removal at different operating conditions. Results showed phosphorous removal efficiencies of 91 and 100% for initial phosphate concentrations of 10 and 1 mg PO_4^{3-}- P/L, respectively. Different isothermal analyses were performed for monolayer and multilayer adsorption processes.

DOI: 10.15376/biores.17.1.975-992

Keywords: Nanocellulose fibers; Nano zero-valent iron; Water pollutants; Flocculants; Climate change; Wastewater management

*Contact information: a: National Research Base of Intelligent Manufacturing Service, Chongqing Technology and Business University, Chongqing 400067, China; b: Chongqing South-to-Thais Environmental Protection Technology Research Institute Co., Ltd., Chongqing 400069, China; c: Sanitary and Environmental Engineering Institute (SEI), Housing and Building National Research Center (HBRC), P. O. Box 1770, Cairo, Egypt; d: Scientific Research Development Unit, Egyptian Russian University (ERU), Badr, Egypt; *Corresponding author: mphdmicro2012@yahoo.com*

INTRODUCTION

Growth and rapid urbanization present the need to search for new technologies that keep water sources safe without any kind of pollution (Abdel-Gawad *et al.* 2016; Mostafa *et al.* 2017; Su *et al.* 2019). The main causes of freshwater pollution can be linked directly to the continued release of coarse toxic industrial waste and effluents. Water sources have different characteristics in terms of water quality. The important factors that affect water quality are organic, inorganic, and biological contaminants (Su *et al.* 2020; Abdelghany *et al.* 2021). Hence, the removal of these pollutants that feed into water systems is a task of concern. Dissolved oxygen (DO), pH, turbidity (NTU), chemical oxygen demand (COD), biological oxygen demand (BOD), phosphorous, and total dissolved salts (TDS) are the most influencing parameters in water quality (Cumbal and SenGupta 2005; Bezbaruah *et al.* 2011; Almeelbi and Bezbaruah 2012; Diallo *et al.* 2013; Mahmoud *et al.* 2021a). The

deviation of these parameter concentrations out of the normal ranges causes water eutrophication, the proliferation of algae, and several diseases to human and aquatic bodies. Water treatment systems depend on different technologies, mainly, adsorption, coagulation, precipitation, and disinfection (Fan *et al.* 2018; Farag *et al.* 2018). Various materials are used in water treatment including coagulants and polymers (Toth 1971; Jayaraman *et al.* 2007; Hill 1910). The effective methodology with low costs, availability, and eco-friendly characteristics is a criterion in sustainable measurements.

Phosphorus represents organic phosphates, orthophosphates, and polyphosphates (Khan *et al.* 1997). The main cause of eutrophication is the increase in phosphorus concentrations. The source of phosphorous could be from phosphate rocks as well as from some solid wastes (Koble and Corrigan 1952; Knight *et al.* 2013). Eutrophication, besides its environmental impact, has some economic merits as a fertilizer (Yuvakkumar *et al.* 2011; Mahmoud *et al.* 2018).

Cellulose is one of the most abundant biodegradable polymers. It has a high effective hydroxyl group ratio. Cellulose consists of repeated β-D-glucopyranose units. Various techniques have been used to prepare nanocellulose fibers, namely cellulose nanocrystals and nanofibrillated cellulose. Plant cellulose is mainly composed of amorphous chains and crystalline domains. Nanocellulose is produced by acid hydrolysis (such as sulfuric, hydrochloric, and phosphoric acids) of the cellulose fibers. Nanocellulose obtained from plants is 5 to 70 nm in width and 100 to 250 nm in length. The type of acids used can affect the colloidal stability of nanocellulose. Nanocellulose can be used as catalytic degradation and disinfection as well as high/ active surface area and high aspect ratio as good flocculants (Mahmoud *et al.* 2019a,b,c). The high mechanical strength of nanocellulose increases stiffness and acid/base resistance, and these attributes give it the possibility for use in different operating conditions. Also, nanocellulose has high surface free energy that can decrease bio-fouling. The adjusting of the medium pH increases the separation of nanocellulose from its colloidal behavior. Many studies have considered the effectiveness of nanocellulose effectiveness for wastewater treatment, including dyes and metal sorption and also the adjacent material in filters and membranes in water treatment systems (Mahmoud *et al.* 2017a,b).

Nanocatalytic materials, such as zero-valence metal, semiconductor materials, and bimetallic nanoparticles, are used in wastewater and water treatment due to their high reactivity and surface area (Meda *et al.* 2007). Several studies have been conducted to study the effect of using magnetic nanocomposites, such as nanocellulose-nano zero-valent iron (NC-nZVI) in the removal of inorganic cations and anions, as well as organic compounds, as shown in Fig. 1 (Almeelbi and Bezbaruah 2012; Mahmoud and Mahmoud 2021b).

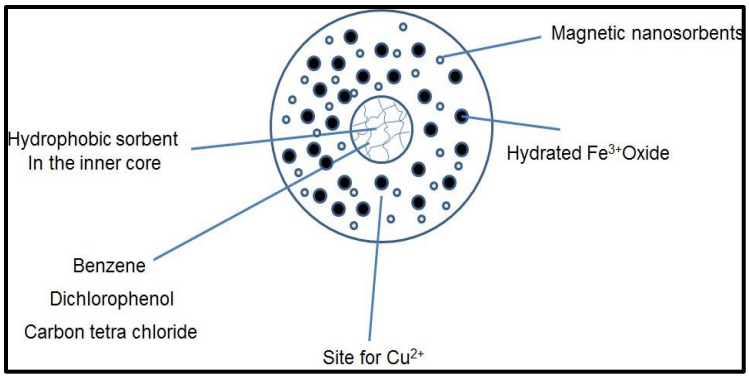

Fig. 1. Contaminants removal behavior by nanocellulose-nano zero-valent iron composite

This paper focused on the use of nanocellulose as a flocculent agent for the treatment of contaminants in water. Nanocellulose was compared with other agents, analyzing nanocellulose removal efficiency of water contaminants and the integrated behavior of NC-nZVI, on phosphorous removal under different operating conditions. Also, the adsorption mechanisms were estimated by applying nonlinear adsorption isotherm models. Finally, regression analysis was employed to detect the response surface relations between the operating variables and removal efficiency.

EXPERIMENTAL

Materials

The materials used in this work included ferric chloride hexahydrate ($FeCl_3.6H_2O$, 98.5% pure, Arabic laboratory equipment Company), sodium borohydride ($NaBH_4$, 99% pure, Win lab Company), ethanol (C_2H_5OH 95%, World Co. for sub & med industries), potassium orthophosphate (KH_2PO_4, 99% pure, ADWIC), sodium hydroxide (NaOH, 99% pure, Oxford co.), sulfuric acid (H_2SO_4, 95-97%, Honeywell), stannous chloride ($TiCl_2$, 99.5% pure, Loba Chem), phenolphthalein, ammonium molybdate (99.9% pure, P.O.C.H., Polska, Poland), ammonium persulphate extra pure, 95.5% pure, Oxford), office paper (source of cellulose).

Methods

Preparation of nanocellulose

Office paper cellulose was pretreated using 2,2,6,6-tetramethyl-1-piperidinyloxy (TEMPO), periodate–chlorite, and 2,3-epoxypropyl-trimethylammonium chloride. Using the sulfuric acid hydrolysis method, nanocellulose fibers were prepared with high colloidal stability because of the presence of sulfate ester groups on their surface.

Preparation of nZVI

Synthesis of nZVI was done using ferric chloride dissolved in ethanol 4:1 (v/v) and sodium borohydride black. Solid particles of nZVI were formed as in Eq. 1 (Bezbaruah *et al.* 2011). To prevent the rapid oxidation of nZVI, washing with absolute ethanol was completed. Finally, the synthesized nZVI was dried overnight at 50 °C (Cumbal and SenGupta 2005).

$$2FeCl_3 + 6NaBH_4 + 18H_2O \longrightarrow 2Fe^0 + 21H_2 + 6B(OH)_3 + 6NaCl \quad (1)$$

Characterization

The prepared NC-nZVI sample was investigated using a Philips Quanta 250 FEG device manufactured by Philips Electronics Company, USA. This was utilized for performing the scanning electron microscopy (SEM) analysis. The SEM instrument operates at a magnification of 80,000x and a voltage of 20 KV. FTIR was analyzed before treatments using FT/IR-6100typeA, S/N A009061020 with a standard light source and TGS detector. The FTIR resolution was 8 cm^{-1}, using a 10000 Hz filter. The SEM and FTIR instruments were located at the National Research Center (NRC). Particle size distribution analysis was conducted for dried samples by using Microvision (particle size measurement) located at CID Company for pharmaceutical industries, Egypt using μ u-tech production, and model VGA-410 France.

Sample collection sites

Samples were collected from contaminated sites in plastic bottles. All analyses were carried out within 8 h of collection at Housing and Building National Research Center (HBRC) laboratories (Cairo, Egypt) (Bezbaruah *et al.* 2011). Three raw water samples were collected. These came from Ismailia Canal, located east of the Delta, at latitude 30°06'41" N and longitude 31°16'22" E, from the Damietta branch at latitude 30°36'15" N and longitude 31°15'39" E, and from a wastewater treatment plant after the primary screens (WWTP) which is located at Helwan Governorate, Egypt.

Batch adsorption studies

The removal efficiency was studied using a batch technique. The concentration of parameters was measured according to (APHA 2017). The sorption percentage was calculated using Eq. 2 and uptake was calculated using Eq. 3.

$$\text{Sorption (\%)} = (C_o - C_e/C_o) \times 100 \quad (2)$$

where C_o is the initial concentration (mg/L) and C_e is the equilibrium concentration (mg/L).

$$q_e \text{ (mg/g)} = ((C_o - C_e)\ V)/\ m \quad (3)$$

where Q_e is the equilibrium adsorption capacity (mg/g), V is the volume of solution (L), and m is the dry weight of the adsorbent (g).

Table 1. Nonlinear Equations of Isotherm Models

Isotherm Model	Nonlinear Equations	Constants		References
Langmuir	$Q_e = \frac{q_m K_a C_e}{1 + K_a C_e}$	K_a	Langmuir constant (L/mg)	(Mahmoud *et al.* 2019a)
		q_m	maximum monolayer adsorption capacity (mg/g)	
Freundlich	$Q_e = K_F C_e^{1/n}$	n	Freundlich constant related to adsorption intensity (dimensionless)	(Mahmoud *et al.* 2019a)
		K_F	Freundlich constant related to adsorption capacity ((mg/g) (mg/L) - 1/n)	
Redlich–Peterson	$Q_e = \frac{K_R C_e}{1 + a_R C_e^{b_R}}$	K_R	Redlich–Peterson isotherm constant (L/g)	(Mahmoud *et al.* 2019a)
		a_R	Redlich–Peterson isotherm constant (1/mg)	
		b_R	Redlich–Peterson isotherm exponent	
Hill	$Q_e = \frac{Q_H C_e^{n_H}}{K_D + C_e^{n_H}}$	Q_H	Hill isotherm maximum uptake saturation (mg/L)	(Fan *et al.* 2018; Moustafa *et al.* 2017)
		K_D	Hill constant	
		n_H	Hill cooperativity coefficient of the binding interaction	
Sips	$Q_e = \frac{Q_s (K_s C_e)^{B_e}}{1 + (K_s C_e)^{B_e}}$	K_s	Sips isotherm model constant (L/g)	(Farag *et al.* 2018)
		B_s	Sips isotherm model exponent	
Khan	$Q_e = \frac{Q_K B_K C_e}{(1 + B_K C_e)^{A_K}}$	Q_k	Theoretical isotherm saturation capacity (mg/g)	(Hill 1910)
		B_k	Khan isotherm model constant	
		A_k	Khan isotherm model exponent	
Toth	$Q_e = \frac{K_t C_e}{(a_t + C_e)^{\frac{1}{t}}}$	K_t	Toth isotherm constant (mg/g)	(Jaroniec 1975)
		a_t	Toth isotherm constant (L/mg)	
		T	Toth isotherm constant	
Koble–Corrigan	$Q_e = \frac{AC_e^D}{1 + BC_e^D}$	A	Koble–Corrigan isotherm constant (Lnmg1−n/g)	(Farag *et al.* 2018)
		B	Koble–Corrigan isotherm constant (L/mg)n	
		D	Adsorption intensity	
Jovanovich	$Q_e = q_{max}\ (1 - e^{K_j C_e})$	Q_{max}	(mg/g) is the maximum uptake	(Jayaraman *et al*. 2007)
		KJ	Javanovic isotherm constant (L/g)	

Isotherm studies

Isothermal studies were performed for the monolayer and multilayer adsorption process using nonlinear equations including the Freundlich, Langmuir, Redlich–Peterson, Hill, Sips, Khan, Toth, Koble–Corrigan, and Jovanovich equations, as shown in Table 1.

Statistical analysis: Response surface methodology

A linear regression analysis was employed to estimate the relation between removal efficiency and operating conditions (pH, dose, contact time, stirring rate, and concentration) on phosphate removal efficiencies as presented in the general equation, Eq. 4. The coefficient of determination statistical measure (R^2 value) was used to evaluate the accuracy of the model. The *t*-test was also used to assess the statistical significance by looking at the p values,

$$Y = \beta_0 + \beta_1 x_1 + \beta_2 x_2 + \beta_3 x_3 + \beta_4 x_4 + \beta_5 x_5 \quad (4)$$

where $Y_{(PO4^{3-})}$ is the predicted response of removal efficiency (%).

RESULTS AND DISCUSSION

Coagulation Efficacy

Treatment of wastewater with NTU 125 and total suspended solids (TSS) 625 (mg/L) was done using different coagulating agents. Measuring turbidity and total suspended solids (TSS) after treatment was done using a jar test mixing rate of 100 rpm for 5 min, 25 rpm for 15 min, and settling for 10 min. Different doses (0.5, 1, 1.5, 2.0, 2.5, and 3.0 mL/L) of 5g/L from each stalk PAC (poly aluminum chloride), polyacrylamide, ferric chloride, aluminum sulfate, and nanocellulose (NC), as shown in Fig. 2.

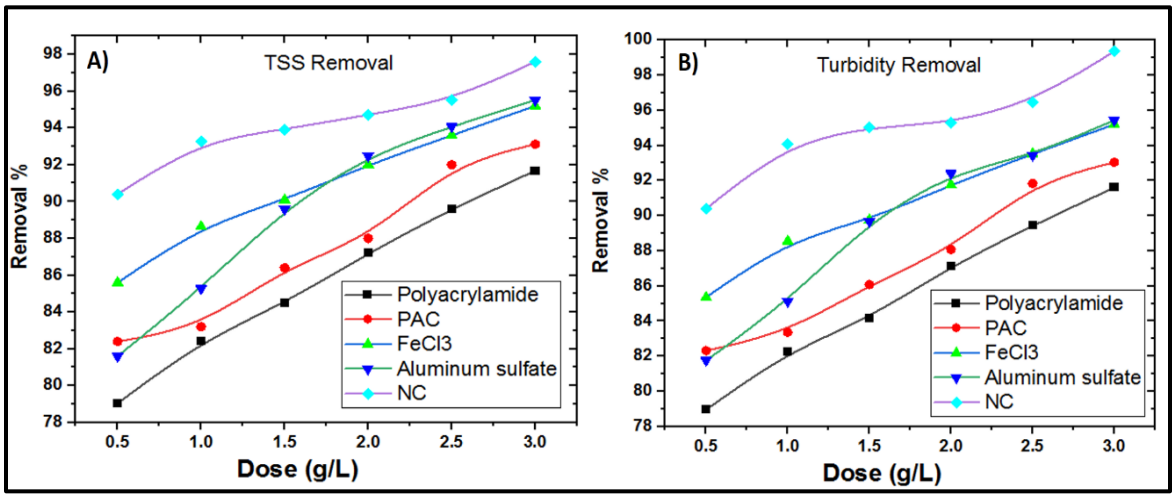

Fig. 2. Effect of different flocculants agents on A) TSS Removal and B) Turbidity removals

Nanocellulose Removal Efficiency of Water Contaminants

Three raw water samples collected from the Ismailia Canal, the Damietta branch, and a wastewater treatment plant were treated using nanocellulose concentration of 5 g/L. These are described in Table 2. The treatment process was carried out within a pH range of 6.7 to 7.4, 100 rpm for 5 min, 25 rpm for 15 min, and settling for 10 min. Results of the

treatment of the Ismailia Canal specimen showed turbidity, COD, BOD, phosphorous, and oil and grease removal efficiency of 96, 83.3,100, 100, and 98.68%, respectively. Results of the treatment of the Damietta branch showed turbidity, COD, BOD, phosphorous, and oil and grease removal efficiencies of 87.5, 81.25, 88.9, 99.11, and 96.38%, respectively. Results of the treatment of the WWTP showed turbidity, COD, BOD, phosphorous, and oil and grease removal efficiencies of 86.36, 91.96, 92.86, 91.74, and 97.18%, respectively.

Table 2. Effect of Nanocellulose on Treatment of Water Samples

Parameter	Ismailia Canal Sample	Damietta Branch Sample	WWTP Sample
Turbidity (%)	96	87.5	86.36
COD (%)	83.3	81.25	91.96
BOD (%)	100	88.89	92.86
TSS (%)	100	85.71	92.13
Phosphorous (%)	100	99.11	91.74
Oil and grease (%)	98.68	96.38	97.18

Integrated Behavior of NC-nZVI, on Phosphorous Removal

Characterization of NC-nZVI

Fourier-transform infrared spectroscopy (FTIR) characterization

Shimadzu S 201 PC spectrophotometer – Tokyo, Japan was used for infrared spectroscopy. The sample was prepared as a disc (2 mg sample + 200 mg spectroscopy KBr). The surface of the NC-nZVI composite had high ratios of OH^- groups that can combine easily with other active functional sulfate esters, carboxyl, amine, and aldehyde groups, as shown in Table 3 and Fig. 3.

Table 3. Indicators of FTIR Observed Bands for NC Sample

IR peak Frequency (Cm^{-1})	Assignment	Transmittance (T) %
713.6	Strong broad N-H amines (RNH2 Or R2NH) or medium =C-H out of plane	46.5
1037.6	Strong C-O stretch (Carboxylic acids or Esters)	44.5
1323.1	Strong C-X stretch Alkyl halides	46.5
1400.2	Medium C-O stretch (RCO-O-H) (Carboxylic acids)	44.5
1527.5	Strong N=O nitroso Or strong N-O asymmetric stretch	41.5
1662.5	C=C Stretch or C=N	41.5
3220.9	Strong broad dimer O-H (Carboxylic acids)	45.5
3400- 3622	Strong O-H free Hydroxyl	43

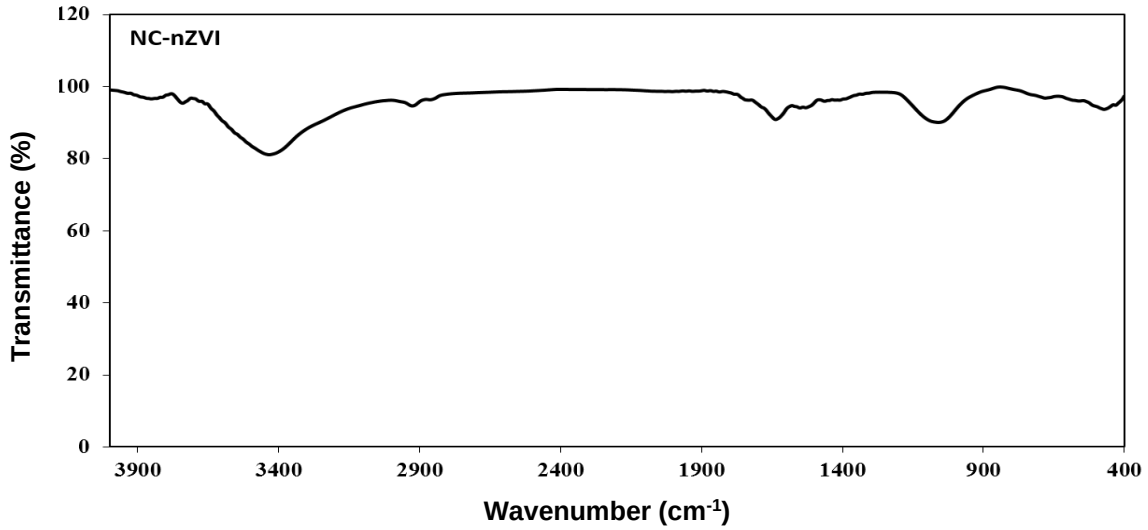

Fig. 3. FT-IR of NC-nZVI powder sample

Scanning electron microscope characterization

The obtained SEM results indicated the formation of Nanocellulose-Nano Zero Valent Iron Composite (NC-nZVI) as fiber with a size ranged between 18 and 26 nm, as shown in Fig. 4.

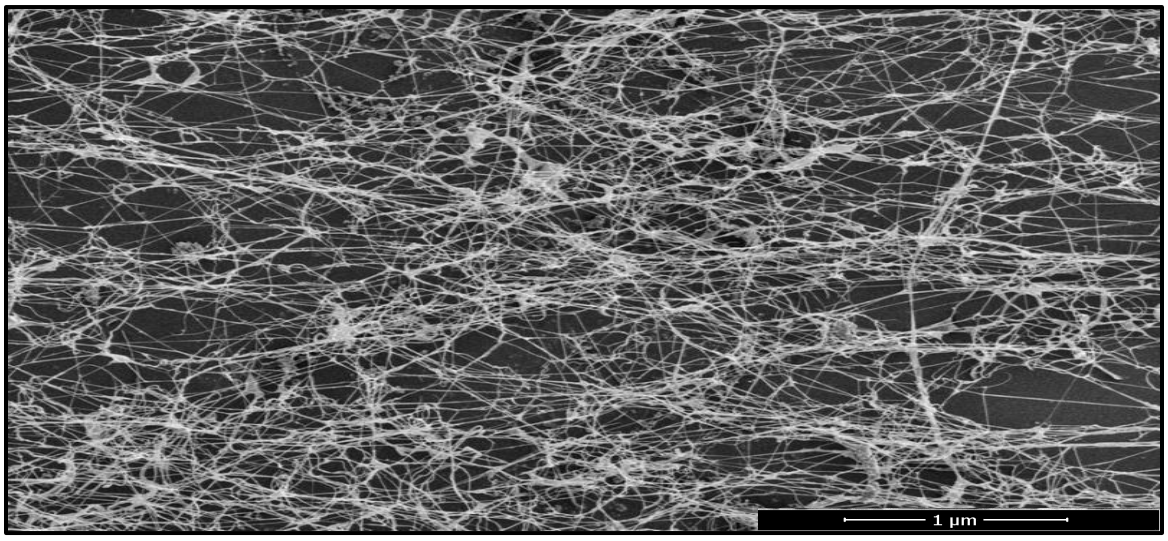

Fig. 4. SEM of NC-nZVI

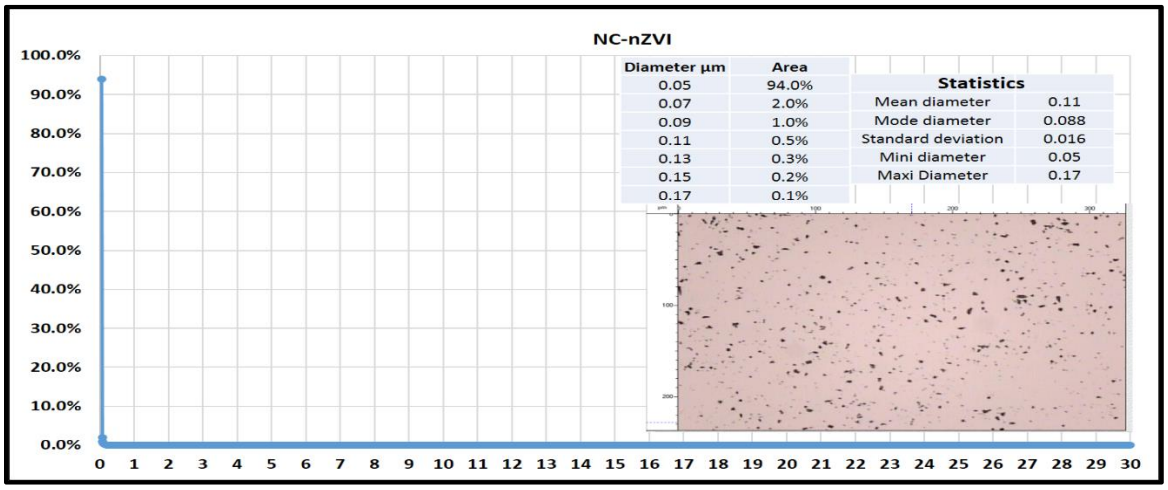

Fig. 5. Particle size distribution of NC-nZVI

Particle size distribution:

Particle size distribution was tested for NC-nZVI from 0 to 30 µm, as shown in Fig. 5. The obtained results indicated that 94% of the prepared NC-nZVI sample was within 50 nm.

Point of Zero Charge (PZC)

The Point of Zero Charge (PZC) was investigated by preparation of 0.1 M KCl, then about 20 mL was adjusted to pH values 2, 3, 4, 5, 6, 7, 8, 9, 10, 11, and 12 by using 1 N H_2SO_4 or 1 N NaOH (pHi) and placed in a 100 mL Erlenmeyer flask. About 0.1 g of NC-nZVI was added into the prepared flasks and left 24 h at 23 ºC. The final pH measurements were determined (pH_f). Averaged values of pH changes after nZVI were obtained from 5 measurements, and all standard deviation values were within ±0.1. The PZC of nZVI was calculated by plotting the relation between ΔpH values (final pH − initial pH_i) and initial pH values (pH_i). The result indicated that the PZC of NC-nZVI was about 7.8, as shown in Fig. 6.

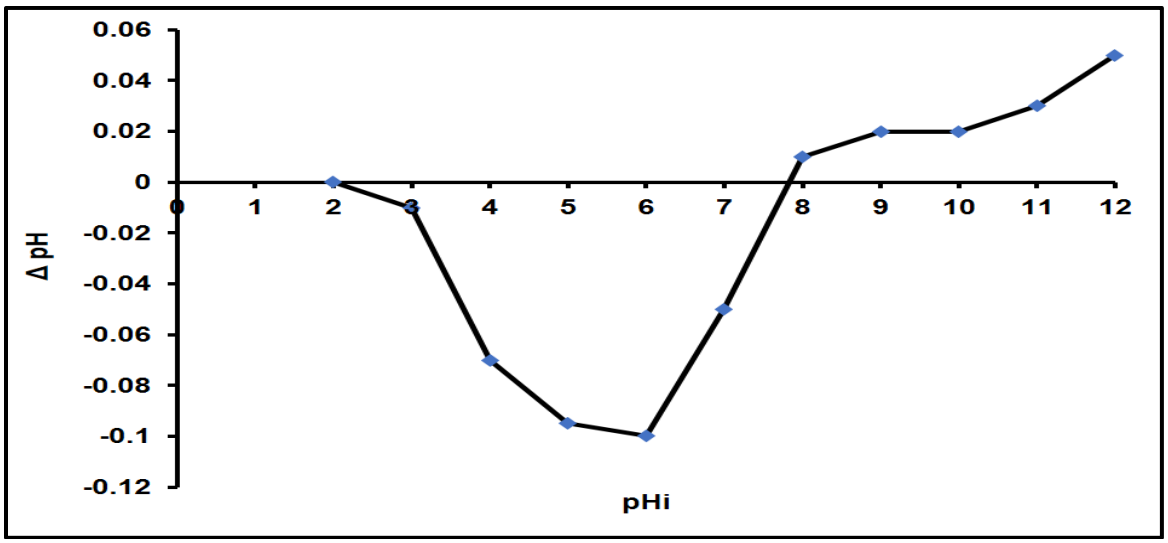

Fig. 6. Point of Zero Charge of the NC-nZVI sample

Effect of Operating Conditions

Effect of pH

The effect of pH was studied at pH 3.5, 4.5, 5.5, 7.5, 8.5, and 9.5 for phosphorous removal by using NC-nZVI. An initial phosphorous concentration of 5 mg/L was used. When the stirring rate was 50 rpm, using 0.2 g/L NC-nZVI with a contact time of 15 min, the removal efficiency was 96, 94, 94, 63, 22, and 22%, respectively for the studied pH values as shown in Fig. 7a. At pH values below the point of zero charge (PZC) of NC-nZVI, the highest efficiency was at pH 3.5 and it decreased significantly at pH higher than 7.3. The PZC for nanoscale zero-valent iron is around 7.7 (Redlich and Peterson 1959). Equations 5 through 9 indicate that the reactivity of NC-nZVI increased below PZC and the efficiency of NC-nZVI decreases in the presence of iron oxide (Ross and Schatz 2014, Mahmoud et al 2021c).

$$Fe_0 + 2H_2O \rightarrow 2Fe^{2+} + H_2 + 2OH^- \quad (5)$$

$$Fe_0 + O_2 + 2H_2O \rightarrow 2Fe^{2+} + 4OH^- \quad (6)$$

$$6Fe^{2+} + O_2 + 6H_2O \rightarrow 2Fe_3O_4\,[\text{magnetite}]\,[s] + 12H+ \quad (7)$$

$$Fe–OH \rightarrow Fe–O^- + H^+ \quad (8)$$

$$Fe–OH + OH^- \rightarrow Fe–O^- + H_2O \quad (9)$$

Depending on the electrostatic repulsion phenomenon, the aggregations increased at PZC and decreased up and down. Also, the accumulation of sorbent materials affect the reactivity due to the decrease in the surface area (Ross and Schatz 2014).

Effect of contact time

The effect of contact time on the phosphorous removal was studied at 5, 15, 30, 60, and 120 min. An initial phosphorous concentration of 5 mg/L diluted from prepared solution (500 mg/L po_4^{3-}-p) was used along with 0.1 g/L from NC-nZVI at a stirring rate of 50 rpm. The removal efficiency was 65, 69, 72, 75, and 73% for the studied contact times, respectively, as shown in Fig. 7b.

Effect of adsorbent dose

The effect of the adsorbent dose was studied at 0.1, 0.2, and 0.3 g for phosphorous removal by using NC-nZVI. An initial phosphorous concentration of 5 mg/L was used. At medium pH 3.5 and stirring rate 50 rpm with a contact time of 15 min, the removal efficiency was 69, 94, and 100%, respectively for the studied NC-nZVI doses as shown in Fig. 7c.

Effect of stirring rate

The effect of the stirring rate on the phosphorous removal was studied at 50, 100, 150, 200, 250, 300, and 350 rpm using an orbital shaker GFL 3018, Prague, Czech. An initial phosphorous concentration of 5 mg/L was used. Using 0.2 g/L of NC-nZVI at medium pH 3.5 with a contact time of 15 min, the removal efficiency was 96, 98, 98, 98, 98, 98, and 98%, respectively for the studied stirring rates as shown in Fig. 7d.

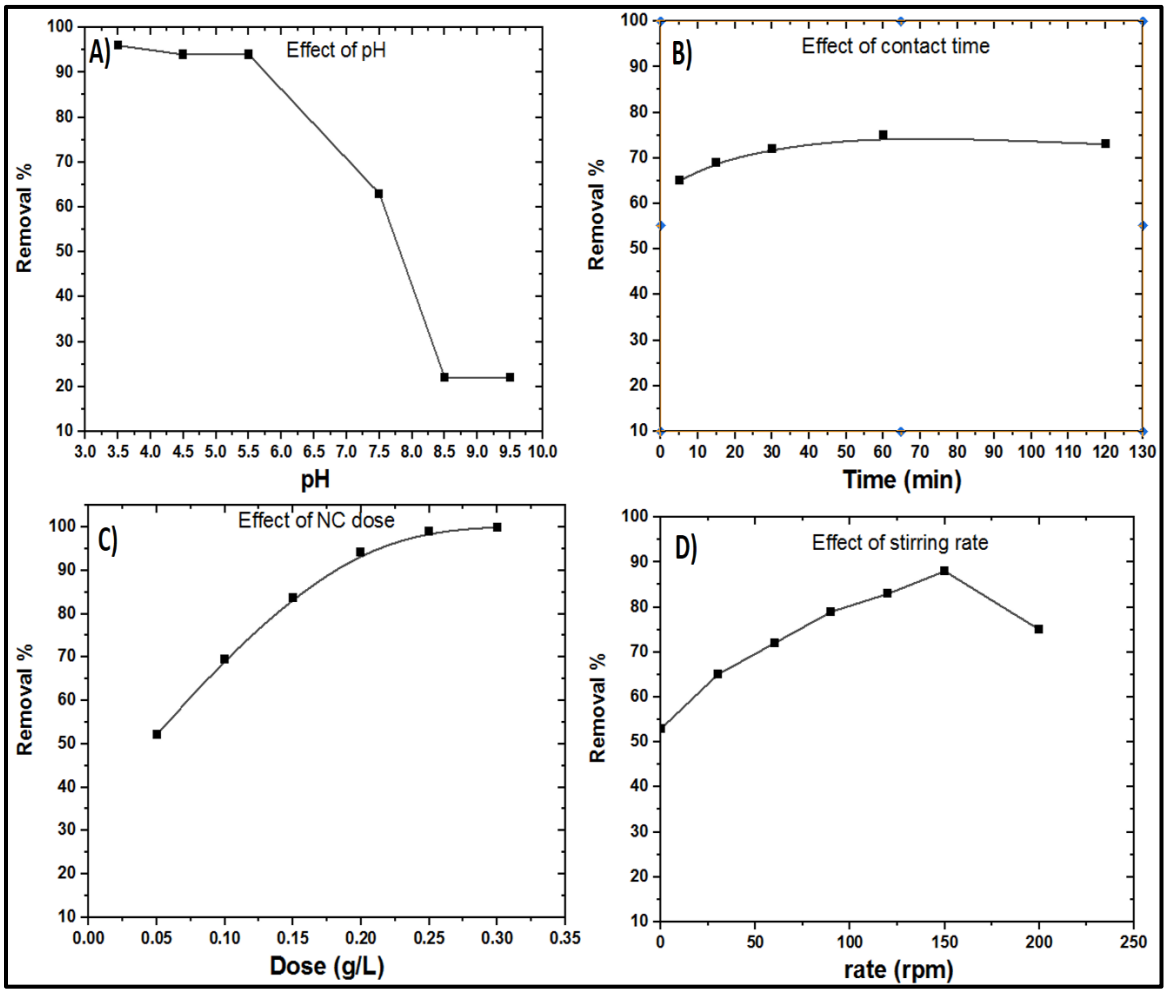

Fig. 7. Effect of operating conditions: A) Effect of pH, B) Effect of contact time, C) Effect of dose, and D) Effect of stirring rate

Effect of the initial phosphorous concentration

The effect of the initial phosphorous concentrations was studied at concentrations 10, 9, 7, 5, 3, and 1 mg/L using NC-nZVI. Using 0.2 g/L of NC-nZVI at medium pH 3.5 and stirring rate 50 rpm with a contact time of 15 min, the removal efficiency was 91, 93.6, 96, 98, 99, and 100%, respectively for the studied phosphorous concentrations as shown in Fig. 8 (Toth 1971; Xi *et al.* 2010).

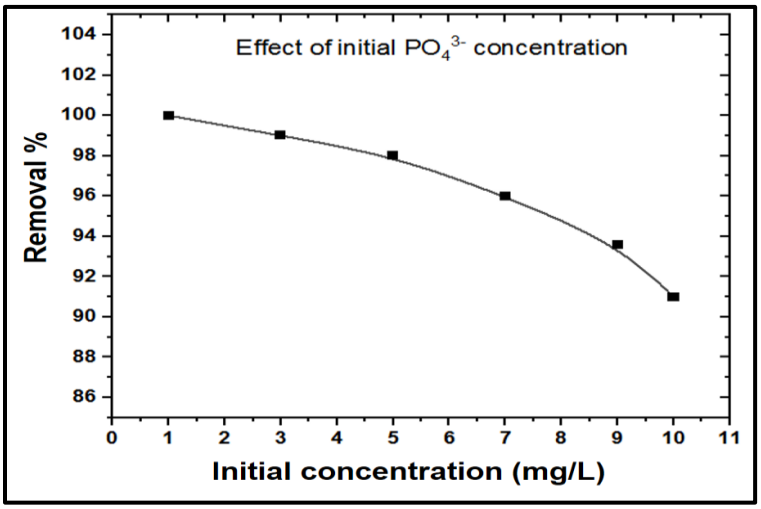

Fig. 8. Effect of initial concentration

Isotherm Analysis

At room temperature, nonlinear relations between isothermal models were considered to describe the removal mechanism, as in Fig. 9. The studied isotherms models were the Redlich-Peterson model, Hill model, Sips model, Khan model, Toth model, Koble-Corrigan model, Javanovic model, Freundlich model, and Langmuir model. The results showed that the NC-nZVI composite was well described by the Sips model (∑ errors: 7.932), as shown in Table 4. The Sips model describes a heterogeneous adsorption isotherm process, which combines Langmuir and Freundlich models. This model tends to approximate the Freundlich model at low concentration and to solve the Freundlich limitation at high concentration through applying the Langmuir adsorption model in the prediction of monolayer adsorption showing the maximum uptake is 105.3 mg (PO_4^{3-})/g (NC-nZVI).

Table (4). Nonlinear Adsorption Isotherm for Phosphate Removal Using NC-nZVI

	Redlich- Peterson		Hill		Sips		Khan		Toth	
Constants	K_r	538.339	Q_H	105.243	Q_s	105.288	Q_k	5.004	K_t	12.425
	B_r	11.181	n_H	0.437	K_s	0.631	B_k	1759.228	a_t	0.089
	G	2339.055	K_D	1.222	B_s	0.437	A_k	0.696	t	3.875
ERRORS										
Chi error	38.452		1.787		0.313		0.364		38.451	
ERRSQ	39.860		3.212		3.212		7.247		39.860	
HYBRD	4.855		0.275		0.275		0.368		4.855	
MPSD	0.843		0.041		0.041		0.032		0.843	
ARE	1.251		0.302		0.302		0.344		1.251	
EABS	13.179		3.789		3.789		6.141		13.180	
Error sum	98.440		9.406		**7.932**		14.496		98.439	

	Koble–Corrigan		Javanovic		Freundlich		Langmuir	
Constants	A	86.103	Q_m	42.275	K_f	48.627	Q_0	48.148
	B	0.817	K_j	8.704	n	3.199	b	11.181
	D	0.437						
ERRORS								
Chi error	0.313		62.207		0.329		38.452	
ERRSQ	3.212		83.163		7.726		39.860	
HYBRD	0.275		7.039		0.347		4.855	
MPSD	0.041		1.005		0.028		0.843	
ARE	0.302		1.498		0.340		1.251	
EABS	3.789		18.187		6.520		13.179	
Error sum	**7.941**		173.100		15.290		98.440	

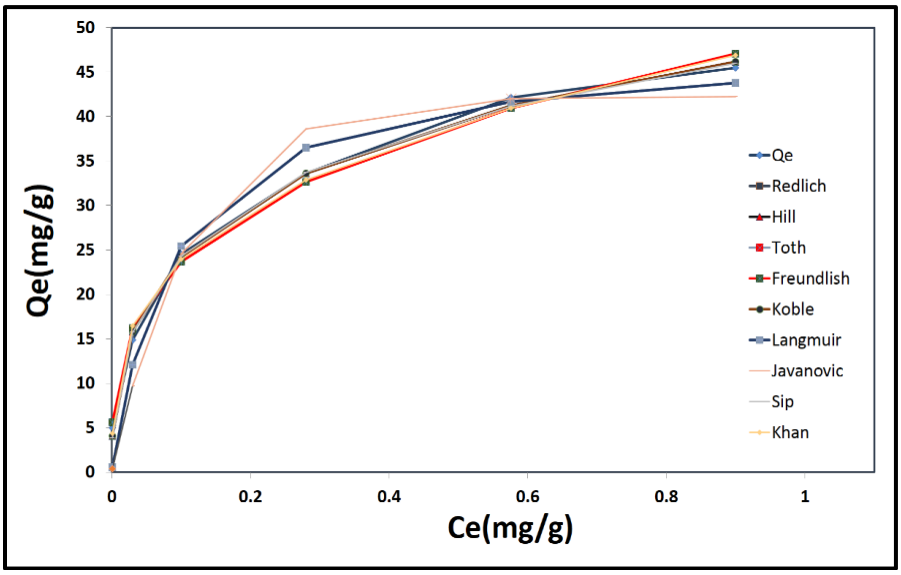

Fig. 9. Adsorption isotherm models for phosphorus removal using NC-nZVI composite. The curve labeled "Qe" corresponds to the experimental data.

Response Surface Methodology (RSM)

Table 5 describes the positive linear effect of the independent variable "pH", and "dose" on phosphate removal was observed to be significant ($p < 0.05$). However, an insignificant effect ($p > 0.05$) was determined for the linear terms of "time", "stirring rate" and "initial concentrations". The coefficient of determination between measured data and simulated results (R^2) and adjusted R^2 existed in Table 5. The significant result of the linear RSM model agrees with the obtained ANN model (Fig. 11) – nonlinear feed-forward backpropagation neural networks – to describe the most significant operating parameters (p-value equal 0.00 for the effect of dose and pH) for phosphate removal using NC-nZVI. By applying Eq. 4, the removal equation appears. The removal equation can be used to control the removal percent by minimizing or maximizing the operating variables using all obtained results not restricted to the optimum conditions,

$$Y = 92.646 - 10.956\, x_1 + 221.112\, x_2 + 0.010\, x_3 + 0.013\, x_4 - 0.813\, x_5 \quad (10)$$

where Y is the predicted response of different wastewater contaminants removal efficiency (%); $x_1$is pH (3.5 to 9.5); x_2 is adsorbent dose (0.1 to 0.3 g); x_3 is contact time (5 to 120 min); x_4 is stirring rate (50 to 400 rpm); x_5 is concentration (1 to 10 mg/L); β_0 is the model intercept; β_1, β_2, β_3, β_4, and β_5 are the linear coefficients of x_1, x_2, x_3, x_4 and x_5, respectively.

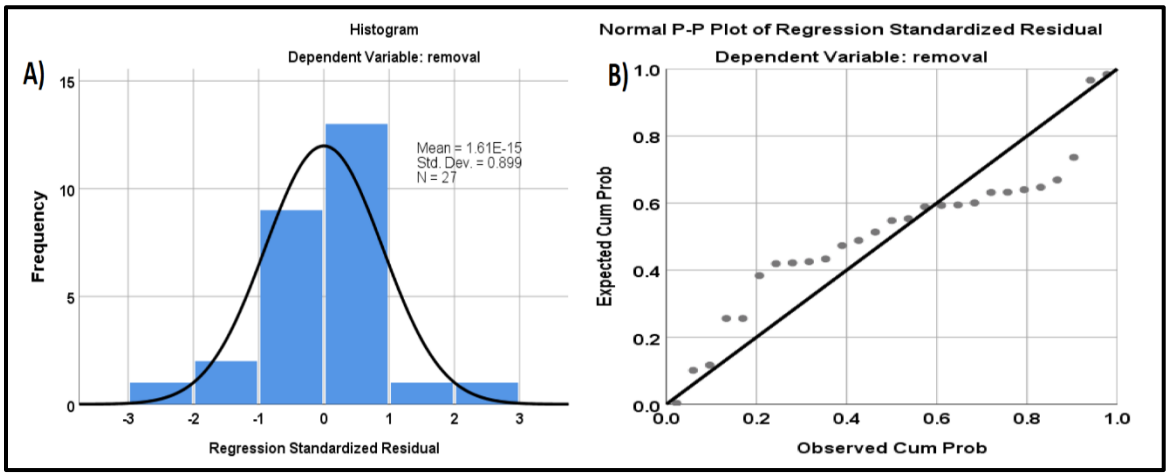

Fig. 10. RSM results for phosphorus removal using NC-nZVI composite A) Histogram, and B) p-p plot

Table 5. t-statistics and p-values for Coefficients of a Linear Regression Model after Using NC-nZVI for Phosphate Removal

		RSM Model (Enter Method)					
Model Summary	**R**	0.961					
	R^2	0.923					
	Adjusted R^2	0.905					
	Std. Error of the Estimate	6.298					
ANOVA	**F**	50.472					
	Model sig.	0.000					
Coefficients		**Term**	**Estimate**	**Standard Error**	**t-Ratio**	**Prob> |t|**	**Effect***
	Constant	β0	92.64	7.9	11.717	0.000	Significant
	pH	β1	-10.956	0.78	-13.9	0.000	Significant
	Dose	β2	221.122	29.5	7.5	0.000	Significant
	Contact time	β3	0.010	0.064	0.16	0.876	Insignificant
	Stirring rate	β4	0.013	0.015	0.83	0.416	Insignificant
	Concentration	β5	-0.813	0.79	-1.03	0.316	Insignificant

Figure 10a describes the histogram plot for the frequency of the residual values (the difference between calculated results and true measurements). The obtained results indicated there was a small deviation between true and calculated values ranging between (-1, +1%) difference indicated the success of Eq. 10 to describe the relation between phosphate removal and operating variables. Also, Fig. 10b demonstrates the linearity of results between expected and observed computational probability.

Finally, Figure 11 describes the importance and normalized importance of each covariable that affect removal efficiency by applying nonlinear statistical algorithms for ANNs expectations.

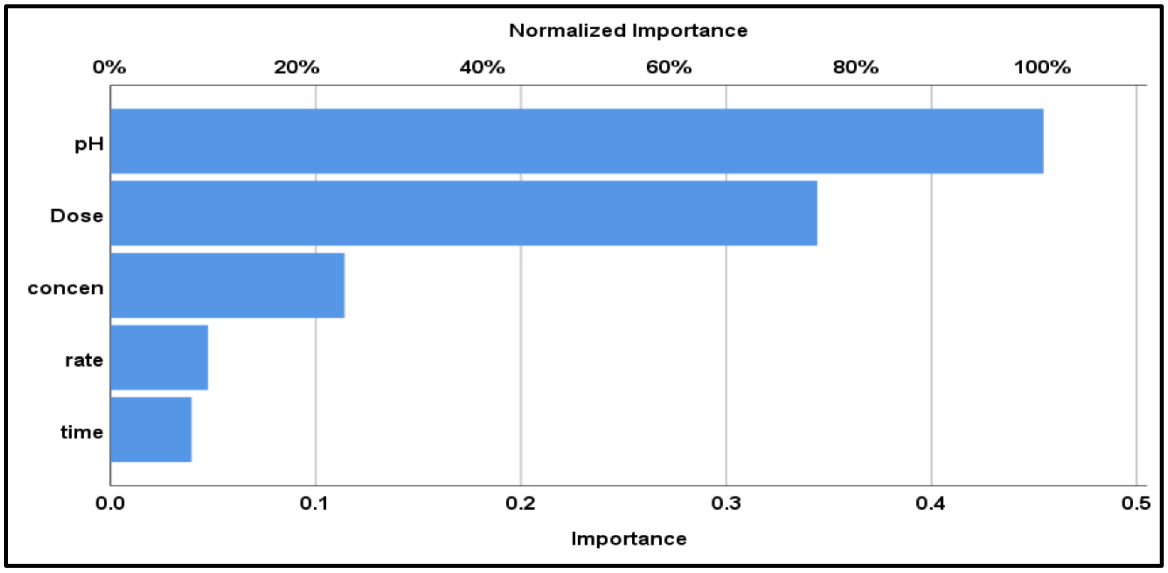

Fig. 11. ANNs: relation between importance and normalized importance for each covariable

CONCLUSIONS

1. The lab-scale model showed effectiveness in phosphorous removal at pH 3.5 using nanocellulose – nano-zero-valent iron (NC-nZVI) composite.
2. Adsorption by the NC-nZVI composite was well described by the Sips model.
3. The NC-nZVI composite proved to be effective for reducing the turbidity, COD, BOD, phosphorous, and oil and grease present in the contaminated waters.
4. The results revealed that NC-nZVI composites could use as good coagulation and adsorbent agent for inorganic contaminants from water sources. Further studies are needed to use the NC-nZVI sorbents as micronutrient fertilizers.

ACKNOWLEDGMENTS

This research was supported by the Science and Technology Research Project of Chongqing Municipal Education Commission (Grant No. KJQN201800831 and KJZD-M202000801). Also, the authors are grateful for the support of the Sanitary and Environmental Engineering Institute (SEI), Housing and Building National Research Center (HBRC), Egypt. Finally, the authors are grateful for complete support from Egyptian Russian University, especially Prof. Dr. Sherif Fakhry Mohamed.

REFERENCES CITED

Abdel-Gawad, S. A., Baraka, M., Elshafai, M., and Mahmoud, A. S. (2016). "Effects of nano zero valent iron and entrapped nano zero valent iron in alginate polymer on poly aromatic hydrocarbons removal," *Journal of Environment & Biotechnology Research* 5(1), 18-28.

Abdelghany, T. M., Mahmoud, M. S., Alawlaqi, M. M., Reyad, A. M., Al-Rajhi, A. M. H., and Abdkareem, E. M. (2021). "Physicochemical characterization of agricultural run-off and groundwater inoculated by *Trichoderma asperellum* and its effect on anti-oxidative enzymes production by irrigated *Trifoliumalexandrinum* L," *BioResources* 16(2), 3272-3284. DOI: 10.15376/biores.16.2.3272-3284

Almeelbi, T., and Bezbaruah, A. (2012). "Aqueous phosphate removal using nanoscale zero-valent iron," *Journal of Nanoparticle Research* 14(7), article no. 900.

APHA (2017). *Standard Methods for the Examination of Water and Wastewater*, 23th Edition, Am. Water Works Assoc. (AWWA), Washington, D.C (2017).

Bezbaruah, A. N., Shanbhogue, S. S., Simsek, S. and Eakalak, K. (2011). "Encapsulation of iron nanoparticles in alginate biopolymer for trichloroethylene remediation," *Journal of Nanoparticle Research* 13, 6673-6681.

Cumbal, L. H. and SenGupta, A. K. (2005). "Preparation and characterization of magnetically active dual-zone sorbent," *Industrial & Engineering Chemistry Research* 44(3), 600-605. DOI: 10.1021/ie040126v

Diallo, M. S., Fromer, N. A., and Jhon, M. S. (2013). "Nanotechnology for sustainable development: Retrospective and outlook," *Journal of Nanoparticle Research* 15, article no. 2044. DOI: 10.1007/s11051-013-2044-0

Fan, S., Mahmoud, M. S., Wen, B., Su, Z., and Zhang, Y. (2018). "Bioelectric activity of microbial fuel cell during treatment of old corrugated containerboard discharges," *BioResources* 13(2), 3545-3553. DOI: 10.15376/biores.13.2.3545- 3553

Farag, R. S., Elshfai, M. M., and Mahmoud, A. S. (2018). "Adsorption and kinetic studies using nano zero valent iron (nZVI) in the removal of chemical oxygen demand from aqueous solution with response surface methodology and artificial neural network approach," *Journal of Environment & Biotechnology Research* 7(2), 12-22.

Hill, A. V. (1910). "The possible effects of the aggregation of the molecules of haemoglobin on its dissociation curves," *Journal of Physiology* 40, 4-7.

Jaroniec, M. (1975). "Adsorption of gas mixtures on homogeneous surfaces extension of Jovanovic equation on adsorption from gaseous mixtures," *Chemical Papers* 29(4), 512-516. DOI:

Jayaraman, K., Anand, K., Chakravarthy, S. R., and Sarathi, R. (2007). "Production and characterization of nano-aluminum and its effect in solid propellant combustion," in: *45th AIAA Aerospace Sciences Meeting and Exhibit 2007*, Reno, NV, USA, pp. 1430. DOI: 10.2514/6.2007-1430

Khan, A. R., Ataullah, R., and Al-Haddad, A. (1997). "Equilibrium adsorption studies of some aromatic pollutants from dilute aqueous solutions on activated carbon at different temperatures," *Journal of Colloid and Interface Science* 194(1), 154-165. DOI: 10.1006/jcis.1997.5041

Knight, M. W. King, N. S., Liu, L., Everitt, H. O., Nordlander, P., and Halas, N. J. (2013). "Aluminum for plasmonics," *ACS Nano* 8(1), 834-840. DOI: 10.1021/nn405495q

Koble, R. A. and Corrigan, T. E. (1952). "Adsorption isotherms for pure hydrocarbons," *Industrial & Engineering Chemistry* 44(2), 383-387. DOI: 10.1021/ie50506a049

Mahmoud, A. S., SaryEl-deen, R. A., Mahmoud, M. S., and Mostafa, M. (2017a). "Adsorption and kinetic studies of using entrapped sewage sludge ash in the removal of chemical oxygen demand from domestic wastewater, with artificial intelligence approach," in: *Conference: 2017 Annual AIChE Meeting*, Minneapolis, MN, USA, https://www.aiche.org/conferences/aiche-annual meeting/2017/proceeding/paper/583aa-adsorption-and-kinetic-studies-using-entrapped-sewage-sludge-ash-removal-chemical-oxygen.

Mahmoud, M. S., Mostafa, M. K., Mohamed, S. A., Sobhy, N. A., and Nasr, M. (2017b). "Bioremediation of red azo dye from aqueous solutions by *Aspergillus niger* strain isolated from textile wastewater," *Journal of Environmental Chemical Engineering* 5(1), 547-554. DOI: 10.1016/j.jece.2016.12.030

Mahmoud, A. S., Mostafa, M. K., and Abdel-Gawad, S. A. (2018). "Artificial intelligence for the removal of benzene, toluene, ethyl benzene and xylene (BTEX) from aqueous solutions using iron nanoparticles," *Water Science and Technology: Water Supply* 18(5), 1650-1663. DOI: 10.2166/ws.2017.225

Mahmoud, A. S., Ismail, A., Mostafa, M., Mahmoud, M. S., Wageh, A., and Shawky, A. M. (2019a). "Isotherm and kinetic studies for heptachlor removal from aqueous solution using Fe/Cu nanoparticles, artificial intelligence, and regression analysis," *Separation Science and Technology* 55(4), 684-696. DOI: 10.1080/01496395.2019.1574832

Mahmoud, A. S., Farag, R. S., Elshfai, M. M., Mohamed, L. A., and Ragheb, S. M. (2019b). "Nano zero-valent aluminum (nZVAl) preparation, characterization, and application for the removal of soluble organic matter with artificial intelligence, isotherm study, and kinetic analysis," *Air, Soil and Water Research* 12, article no. 1178622119878707.

Mahmoud, A. S., Mostafa, M. K., and Nasr, M. (2019c). "Regression model, artificial intelligence, and cost estimation for phosphate adsorption using encapsulated nanoscale zero-valent iron," *Separation Science and Technology* 54(1), 13-26. DOI: 10.1080/01496395.2018.1504799.

Mahmoud, A. S., Mohamed, N. Y., Mostafa, M. K. and Mahmoud, M. S. (2021a). "Effective chromium adsorption from aqueous solutions and tannery wastewater using bimetallic Fe/Cu nanoparticles: response surface methodology and artificial neural network," *Air, Soil and Water Research* 14, 1-14. DOI: 10.1177/11786221211028162.

Mahmoud, M. S., and Mahmoud, A. S. (2021b). "Wastewater treatment using nano bimetallic iron/copper, adsorption isotherm, kinetic studies, and artificial intelligence neural networks" *Emergent Materials*. DOI: 10.1007/s42247-021-00253-y.

Mahmoud, M., Mahmoud, A. S., El-Said, M. A., and Mostafa, M. K. (2021c). "Comparison of aluminum and iron nanoparticles for chromium removal from aqueous solutions and tannery wastewater, empirical modeling and prediction," *Emergent Materials*, 1-16.

Meda, L., Marra, G., Galfetti, L., Severini, F., and DeLuca, L. T. (2007). "Nano-aluminum as energetic material for rocket propellants," *Materials Science and Engineering: C* 27(5), 1393-1396. DOI: 10.1016/j.msec.2006.09.030

Mostafa, M. K., Mahmoud, A. S., Saryel-Deen, R. A., and Peters, R. W. (2017). "Application of entrapped nano zero valent iron into cellulose acetate membranes for domestic wastewater treatment," 2017 Annual AIChE Meeting; Minneapolis, MN, October 29 - November 3, 2017.

Redlich, O., and Peterson, D. L. (1959). "A useful adsorption isotherm," *Journal of Physical Chemistry* 63(6), 1024-1024. DOI: 10.1021/j150576a611

Ross, M. B., and Schatz, G. C. (2014). "Aluminum and indium plasmonic nanoantennas in the ultraviolet," *The Journal of Physical Chemistry C* 118(23), 12506-12514. DOI: 10.1021/jp503323u

Su, Z., Fan, S., Zhang, Y., Tian, C., Gong, C., Ni, J., Yang, B., Peng, F., Korkko, M., and Mahmoud, M. S. (2020). "Industrial scale-up of fiber recovery technology from mixed office waste fine screen reject," *BioResources* 15(3), 6420-6430. DOI: 10.15376/biores.15.3.6420-6430

Su, Z., Mahmoud, M. S., Fan, S., Zhang, Y., and Peng, F. (2019). "Combustion properties of mixed black liquor solids from linter and reed pulping," *BioResources* 14(4), 8278-8288. DOI: 10.15376/biores.14.4.8278-8288

Toth, J. (1971). "State equations of the solid-gas interface layers," *Acta Chim. Acad. Sci. Hungar.* 69(3), 311-328.

Xi, Y., Mallavarapu, M., and Naidu, R. (2010). "Reduction and adsorption of Pb^{2+} in aqueous solution by nano-zero-valent iron—a SEM, TEM and XPS study," *Materials Research Bulletin* 45(10), 1361-1367. DOI: 10.1016/j.materresbull.2010.06.046

Yuvakkumar, R., Elango, V., Rajendran, V., and Kannan, N. (2011). "Preparation and characterization of zero valent iron nanoparticles," *Digital Journal of Nanomaterials and Biostructures* 6(4), 1771-1776.

Article submitted: October 3, 2021; Peer review completed: November 30, 2021; Revised version received and accepted: December 10, 2021; Published: December 15, 2021.
DOI: 10.15376/biores.17.1.975-992